

Chapter 4

Electrical Impedance Tomography to Detect Trends in Pulmonary Oedema



Franco Simini, Eduardo Santos, and Martín Arregui

4.1 Introduction

Electrical impedance tomography (EIT) has evolved over the last four decades since the Sheffield pioneering works (Barber and Brown 1984) until present-day clinical equipment. The ability to obtain “slices” of parts of the body non-invasively is what makes EIT so attractive despite its relatively slow development and limited adoption in clinical settings. As described in the chapter by Bayford, EIT employs harmless currents with no physiological nor functional consequences on the patient. If one compares the high-definition anatomical details available in present-day computer tomogram (CT) scans, magnetic resonance imaging (MRI) or even positron emission tomography (PET) images—which all involve hundreds of processed radial attenuation signals—with the result of a series of 16 electrodes applied on the patient’s skin for high-frequency current injection and voltage measurement, elementary concepts of signal analysis theory imply that EIT is not competitive in terms of accuracy. This is because paired combinations of 16 measurement points are outnumbered by the thousands of pixels available in the other imaging techniques.

Although complex inverse problems are mathematically tackled in EIT making a number of theoretical assumptions, the tomographic images with colour-coded conductivity are secondary to a limited data set and therefore have a relatively modest information content. Since air and water have very different resistivities, water can be spatially distinguished from air, with the potential to give clinicians a powerful tool to monitor and record the presence of both elements in body segments of critical patients where there should be only air, such as the airways and alveoli.

F. Simini (✉) · E. Santos · M. Arregui
Núcleo de Ingeniería Biomédica de las Facultades de Medicina e Ingeniería, Universidad de la República, Montevideo, Uruguay
e-mail: simini@fing.edu.uy

In this chapter we discuss the strength of EIT over other imaging techniques, based upon its fundamental “weakness”, i.e. giving only “rounded-up figures” of air/fluid occupation, without high anatomical accuracy, at a much lower price in terms of costs, untoward effect of ionizing radiation (CT or PET) or size of the equipment (MRI). EIT is a low-cost, non-invasive, continuous measurement method used to obtain images of the distribution of pleuropulmonary fluids and air.

Estimation of alveolar fluid content and distribution is essential in the management of conditions such as cardiogenic pulmonary oedema, pleural effusions, pneumonia and acute respiratory distress syndrome (ARDS). Electrical impedance of tissues can be estimated by measuring voltages on the skin while applying high-frequency currents whose amplitudes are far below perception thresholds. Processing electrical impedance matrices yields tomographic images (Barber and Brown 1984).

This chapter (1) reviews the basic concepts of EIT with emphasis on precision and consistency which are related to the potential of becoming a clinical monitoring technique; (2) shows design decisions made by several authors, comparing them to existing commercial devices with similar characteristics; and (3) describes the main features of an EIT prototype as a starting point for interested readers and developers.

4.2 Physics and Clinical Wish List

The behaviour of water and air differs greatly with respect to ionic current travelling through them. Different tissue types or different tissue physiopathological conditions also react differently to the passage of electrical current. The electrical current in man-made conductors turns into ionic displacements in biological tissue; the electrodes are the key factors of our measurement capacity. This physical property suggests that an instrument capable of displaying the relative content of air and tissue in the thorax could be clinically useful. If in addition the geometrical distribution of air-filled alveoli and fluid-filled alveoli was drawn, then a practical evaluation tool could be devised. In case the processing time of such inner distribution was quick enough, we would have a suitable monitoring equipment. The injection of high-frequency current (>20 kHz) at amplitudes not perceived by the human body (of the order of a few mA) and the resulting measurements of voltages on the chest's skin allow to estimate the electrical impedance. This estimation can be displayed as a tomographic image, by applying one of a set of possible reconstruction techniques.

Treatment of pulmonary oedema is based, among other clinical parameters, upon the estimation of alveolar volume occupied by liquid. This estimation of the fluid occupation of the chest would be greatly facilitated by the availability of a graphical representation of its size and density to guide therapeutic interventions. Currently the clinician has only indirect estimations because X-ray imaging or computed tomography cannot be performed often enough, due to the difficulties of repeatedly carrying patients to radiological facilities and to the limitations imposed

by the side effects of ionizing radiations. EIT is a promising alternative to moving critically ill patients and at the same time gives continuous information. Following the publications of several research groups in the 1980s, the Nucleo de Ingenieria Biomedica (nib) has developed since 1995 a number of circuits (Ferreira et al. 2002), tomographic reconstruction software products (Hartman et al. 2002) and prototypes (Gonzalez et al. 2005; Quinteros and Simini 2007; Santos and Simini 2012) under the name of IMPETOM (IMPEdance TOMography Montevideo) with test results in phantoms and healthy volunteers.

Circuit designs for EIT are reviewed, including wave generators, current sources, differential amplifiers, synchronous voltmeters, multiplexers and control modules. Nine designs are studied; the characteristics of five of them are presented (England 2005, Uruguay 2002, Iran 2006, China 2007 and Switzerland 2012). Three different solutions are compared, and an optimal design is proposed which includes a direct digital synthesizer (DDS) for signal generation, a modified Howland configuration for current source, 16 bits for the analog-to-digital conversion and a digital signal processor (DSP) for the synchronous demodulation as well as to process the measurements for the reconstruction algorithm. This allows us to design low-cost, gross graphical representations for oedema extent monitoring, with little anatomical accuracy. It is important for physicians to have a real-time representation, over time (hours and days), of the trend in fluid accumulation in the lungs. Figure 4.1 shows a colour-coded representation of normal lungs, detected by an EIT system.

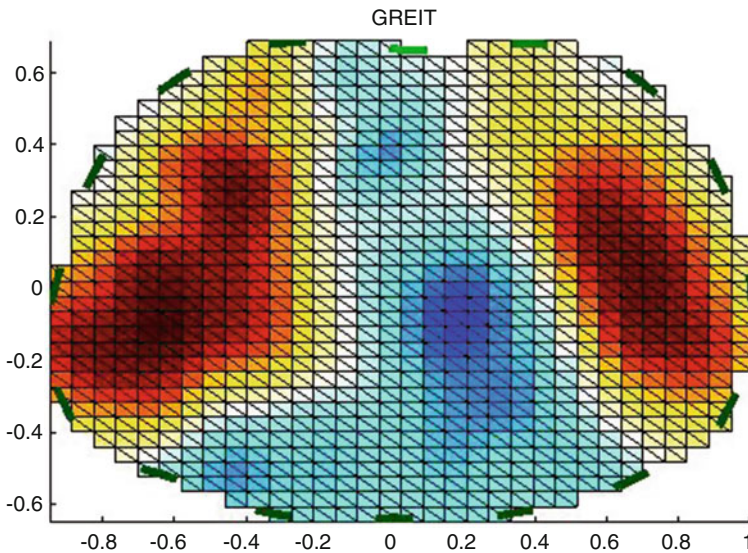


Fig. 4.1 EIT representation of normal lungs. Red is high bioimpedance, yellow is intermediate impedance, and blue is low impedance, i.e. organs and tissues. Taken from Santos (2014) with permission

4.3 Hardware Architecture

The main blocks of an EIT system, (1) waveform synthesis, (2) current source, (3) differential amplifier, (4) synchronous voltmeter, (5) multiplexers and (6) control circuitry, are shown in Fig. 4.2.

Waveform Synthesis The waveform generator creates the reference signal for the sinusoidal current source, besides generating the synchronizing signal to be used by the demodulator. There are analog and digital solutions; the latter is the most commonly used like in the circuit described by Saulnier (2004). This is followed by a digital-analog converter with stored samples. The performance of waveform synthesis is measured in terms of spectral purity and its signal-to-noise ratio (SNR).

Current Source The current source is driven by the waveform generator signal to convert it into a current to be injected into the body through the electrodes. Either single-ended or floating input can be used; the former is appropriate for multiple-source systems, while the latter configuration is best adapted to single-source systems (Saulnier 2004). All current source designs published (discrete op amps or transistors) face the same problem: i.e. output impedance is difficult to be kept high (Saulnier 2004). This impedance consists of an output resistance and stray capacitance: the output impedance thus affects the value of the injected current, depending on the load seen by the source, in this case the human body (including the electrode/skin interface), which is constantly changing. That is why the design of the source must take into account load variability in order to obtain an output impedance that allows the current to vary at most within the A/D least significant bit (Saulnier 2004).

Differential Amplifier Either differential or single-ended voltages may be measured in principle, but the vast majority of systems include differential configurations, with as a consequence a reduced voltage dynamic range (Saulnier 2004). Designers face here a second problem: the common-mode voltage of the amplifiers. To reduce it, the components and the operating point must be chosen very carefully. In addition to this, one may use specific techniques, such as an additional electrode

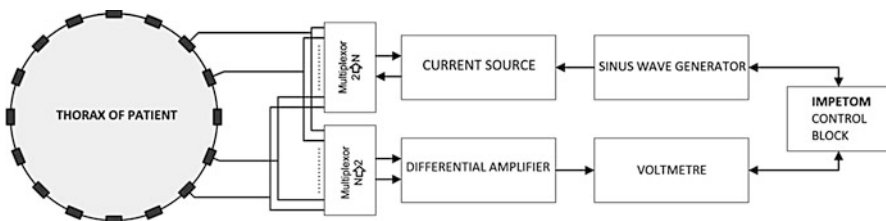


Fig. 4.2 EIT system structure with typically 16 electrodes affixed onto the skin of the patient's body. After Santos (Santos and Simini 2013) with permission

located away from the area where the measurement is taken to feedback a “driven-right-leg” current much in the same way as in ECG circuits (Webster 2010).

Synchronous Voltmeter To reconstruct a tomographic image, it is necessary to take phase-sensitive voltage measurements, either to measure the resistivity and permittivity or just the resistivity. This is why it is necessary to have a coherent signal from the wave generator. This demodulation can be either in the analog or digital domain; the latter is the most used recently (Saulnier 2004). One way to perform the digital demodulation is multiplying the A/D-converted input by a cosine function of the same frequency, and the samples are then integrated over a number of cycles of the original wave.

Multiplexers Multiplexers are needed in systems with a single current source or with fewer voltmeters than electrodes. Multiplexers are used to select channels through which current is injected and/or where the voltage is measured. Multiplexers have nonideal characteristics and exhibit, for instance, an “on-resistance” which distorts the desired signal and, above all, introduces input and output capacitances.

Control and Data Storage Block Control is necessary to synchronize all other blocks, to store the measured data and to transfer it to a computer that will perform the image reconstruction. Possible designs span from basic microcontroller (Xu et al. 2005) to high-performance digital signal processors (DSPs) (Xu et al. 2005; Wang et al. 2005a, b; Hamidi et al. 2010) to include more complex data preprocessing before computer involvement.

4.4 Review of EIT Systems

Several authors have published original work on EIT hardware systems, some of which are described here. A great variety of technical solutions are presented, giving the reader hints for personal developments.

Ferreira et al. (2002) proposed an EIT circuit with sinusoidal signal generation using the function generator MAX038 (Maxim). The current source includes the operational amplifier AD844 (Analog Devices). Two multiplexers MAX336 (Maxim) select the electrodes that carry the current. In the measurement stage, 16 identical circuits avoid the use of a multiplexer. The INA114 (Burr-Brown) operates as an instrumentation amplifier, and its output is fed to a bandpass filter made with the MAX274 chip (Maxim). A sample and hold circuit captures the filter output with the LTC1043 (Linear Technology) IC.

González et al. (2005) used the PC-LPM-16PnP (National Instruments) board as control stage, with 16 A/D 12-bit conversion input channels. The results measured show a SNR (signal-to-noise ratio) of 40 dB, a CMRR (common-mode rejection ratio) of the order of 50 dB and a current source output impedance of 560 k at 50 kHz.

Wang et al. (2005a, b) used a TMS320F206 (Texas Instruments) DSP for control and data preprocessing. A voltage-controlled current source (VCCS) generates the signal that is injected by the electrodes. To measure voltages, a multiplexer is implemented with the AD734 (Analog Devices) IC, a low-pass filter with MAX275 chip (Maxim) and AD1674 (Analog Devices) converter, reaching a rate of 30 frames per second.

Soleimani (2006) designed a low-cost equipment where the waveform is digitally generated using a 23 kHz stored sinusoid in an EPROM (27C258), fed to a D/A converter (DAC-0808 National Semiconductor). 1.3% of harmonic distortion was measured. The signal is fed to a buffer which in turn is connected to a VCCS, (implemented using AD644 by Analog Devices). To measure voltages, a synchronous demodulator is used due to its ability to remove noise. An AD625 instrumentation amplifier (Analog Devices) is included as input stage to be fed to the PCL-812PG I/O (Advantech) board.

Xu et al. (2005) created a system using 128 electrodes for three-dimensional (3D) images of the human thorax. A multiple frequency current (1 kHz–2 MHz) is injected using the IC AD9852 (Analog Devices). The control module is implemented with TMS320F2812 (Texas Instruments). The multiplexer is a MAX306 (Maxim). Data acquisition is done by AD624 (Analog Devices) used as a preamplifier, followed by a fourth-order Butterworth filter (MAX275 by Maxim). The synchronizing signal (AD9852) is used in the DSP to implement the synchronous demodulator. Reconstructed images are shown, but no SNR nor any other performance figures are given.

Bera and Nagaraju developed in 2009 (Bera and Nagaraju 2009) a system to study calibration issues. For current injection they use a voltage-controlled oscillator (VCO) built with the MAX038 (Maxim), which feeds a modified Howland-type current source (Saulnier 2004). This module is constructed with two operational amplifiers AD811 (Analog Devices) and generates a current of 1 mA at 50 kHz. A differential amplifier stage and filter is used for the voltage measurement with a multimeter and a digital oscilloscope. A central electrode is used to reduce the common-mode signal. Command mode is reduced at best to 67 mV.

Hamidi et al. implemented in 2010 (Hamidi et al. 2010) a synchronous demodulator with a DSP (Texas Instruments MS320C6713) which is mounted on the development board TLV320AIC23 (Texas Instruments). This board has two 16-bit ADCs (AIC23 Texas Instruments) 96 kbps sampling rate. With simulated data, the system had a phase error of 0.12° and a signal-to-noise ratio (SNR) of 130 dB.

Gaggero et al. (2012) developed a system to address two important problems affecting EIT reliability and usability: (a) electrode contact impedances, large and varying due to movement, and (b) placing of the electrodes for each individual patient. To solve these problems, Gaggero implemented a method of active electrodes, which uses a voltage buffer in the proximity of the electrodes to stabilize the contact impedance. A multiplexing method reduces the length of wires from the electrode belt to the central block. The signal generator, the power source, the electrode handling and the communication with the PC are in the central block of the equipment. Two standard boards are used for this: an Altera Stratix II Development

Kit (Altera) which includes both AD9433 ADC (TI) and DAC904 DAC (TI) and an Ethernet interface. A custom developed board is responsible for the analog stage, with differential amplifier and high-pass filter implemented with an AD8221 (Analog Devices), signal conversion into a differential signal and low-pass filtering (THS4502 by TI). The sinusoidal signal is generated in the FPGA by a numerically controlled oscillator (NCO) and a modified Howland current source.

Dixtal Biomedical developed a commercial system DX 1800, seen in operation in Montevideo in 2010, which provides real-time EIT chest images. It has two modules: the DX1800 itself and a monitoring software that runs on a computer. The DX 1800 has 32 electrodes to be placed around the patient's chest. The software handles the user interface and displays the reconstructed chest images.

PulmoVista 500 was first introduced by Dräger Medical (2011) to display lung ventilation in real time. A very practical belt with 1 row of 16 electrodes is placed around the chest and injects currents between 80 and 130 kHz, generating images at a rate of 10–30 per second with 1440×900 pixel resolution.

Santos in 2014 (Swisstom) suggested to use standard evaluation boards for an efficient EIT system design, as described in the following paragraph.

Alfaro et al. (2015) and Arregui et al. in (2016) and 2016 include an “RC phantom” in the design of an EIT system, as a calibration feature for both development time and normal use.

4.5 Suggested Design Options

After our own and projects by others (which we just reviewed), there are three possible options for EIT hardware: one is a completely analog signal processing design, and the other two solutions use a DSP, and decisions depend upon cost factors, building difficulty, performance and speed.

4.5.1 Discrete Components with No Digital Processing

The first option is to design using discrete components without a DSP, but with a basic microcontroller (e.g. ATmega168, Atmel, costs \$3, the one used in Arduino boards) which would be responsible for control and synchronization of the remaining blocks. Signal demodulation would be carried out using discrete components, as well as filtering and amplification. An A/D converter would be used to send signals to the computer for image reconstruction. A precaution for improving system performance would be to use at least 16-bit ADC resolution. The data acquisition cards (DAQs) have multiple input channels, making it possible to have a separate channel for each pair of electrodes, enabling measurements in parallel. This also means to have to build 16 input channels (same as IMPETOM C (Ferreira et al. 2002)), increasing the cost and difficulty of design. A DAQ with several input

channels is expensive, such as the NI USB-6211 by National Instruments (approx. \$690). The main problem with this solution is electrical noise, which is difficult to reduce, as well as the imperfection of discrete electronic components that dominate the design giving in the end poor reconstructed images. The advantage of this option is its low cost, except for the expensive DAQ included.

4.5.2 Standard Evaluation Board

To minimize signal processing in analog form, and thus noise interference, A/D conversion must be included in the design as near as possible to the measurement point. As much processing as possible is performed in digital format, including basic first filtering and gain stages, using a DSP standard evaluation board. Demodulation is also done in the digital domain. This option gives great processing flexibility, in terms of giving designers the possibility to obtain both resistivity and permittivity measurements, in addition to reducing discrete component-originated errors. By using a DSP board, the measurement vector ready to be used in the reconstruction is transmitted to the computer.

Examples of boards are the Starter Kit TMS320C6713 (IT, \$ 395) or the Evaluation System ADSP-BF533 EZ-Kit (Analog, \$ 490). Despite that these boards are limited, the advantage of using them is that of shortening prototype development time because they are complete systems with DSP, memory, demodulators, A/D with programmable gain amplifiers (PGAs), communication with the computer, ports for general use as well as a circuit to program the DSP. Figure 4.3 shows the block diagram for a system implemented with an evaluation board.

The disadvantage is that standard boards have a fixed set of components, some of them not suited to solve the problem faced. Most of these cards, at least those found in a price range between \$300 and \$600, are designed to work with audio, and therefore the A/D and PGAs are available within a codec (Alfaro et al. 2016) specifically designed for audio processing. The most notorious limitation is that codecs operate at frequencies used in standard audio, the higher sampling frequency being 96kSPS (samples per second). According to the Nyquist theorem, a maximum limit for our EIT frequency left is 48 kHz, which is not enough to get good SNR values, because the operating frequency available in practical design turns out to be below 20 kHz, due to the several simultaneous tasks. A pity considering the DSP within the TMS320C6713 board has the potential to operate at 225 MHz and to perform 1350 million floating-point operations per second (MFLOPs) (Alfaro et al. 2016). Another disadvantage is the relatively high cost.

4.5.3 Discrete Components with Digital Processing

To overcome the limitations of using a Starter Kit, we have the option to work with DSPs and to choose the components that are most suited to our problem. The use of DACs with a higher sampling frequency, such as the AD7892 (Analog, \$ 23)

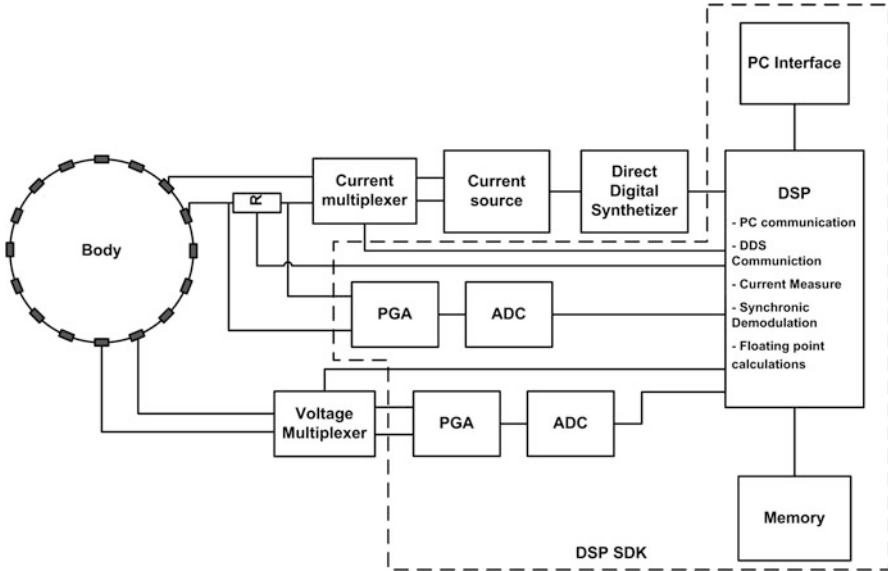


Fig. 4.3 EIT design using an evaluation board. After Santos and Simini (2012), with permission

which has 18 bits of resolution and the ability to get up to 1MSPS, which would theoretically allow us to work up to a frequency of 500 kHz. The advantage of a lower cost is greatly offset by the difficulty to achieve a truly compatible and harmonious design (including clock speed, type of communication, supply voltages) as well as to assemble in the laboratory successive working prototypes (component layout, soldering techniques, handling).

4.5.4 Suggested Design

The proposed design for IMPETOM improves over previous implementations, overcoming the most outstanding problems by digitizing the signals in early stages. By doing this we can take advantage of the precision of digital filtering and demodulation. Our suggested design is based on an evaluation board, such as OMAP-L137/TMS320C6747 Floating-Point Starter Kit (\$ 415, Spectrum Digital). The most important characteristics are the inclusion of an OMAP-L137 processor, with a C6747 VLIW DSP floating-point processor and an ARM926EJ-S processor operating up to 300 MHz, 64 MB SDRAM, USB2 2.0 interface, TLV320AIC3106 stereo codec and expansion connectors for daughter cards.

The codec has four input channels, and considering that a channel will be used to measure the injected current, there would be three input channels available to measure voltages in parallel. This system enables to perform two significant

improvements over previous systems (Ferreira et al. 2002; Gonzalez et al. 2005; Quinteros and Simini 2007):

1. To measure the injected current with a digital metre controlled by the control block which ensures that the signal obtained makes the most of the range of the ADC.
2. To have a single voltage measurement channel with a multiplexer. Despite the increased acquisition time (due to parallel channels read in sequence) and the multiplexer sources of noise and errors (Saulnier 2004), this change reduces the complexity and cost of 16 measuring channels of the IMPETOM project (Ferreira et al. 2002).

4.6 Inverse Problem

4.6.1 *Mathematical Background*

Since EIT is a technique used to derive conductivity within a region from measurements taken on its boundary, the region of interest is the space delimited by the patient's skin. The same electrodes used to inject currents are also used to measure voltages as "boundary conditions", i.e. the contour of what the technique is interested in. There are several possible configurations for an EIT system, including a variety of frequencies and waveforms of injected currents, the number of electrodes and their positioning, e.g. adjacent or opposite electrodes described elsewhere in this book and within this chapter. The problem to solve when extracting information from the unknown "inside" from data measured on the border is essentially a mapping problem. In very much the same way as cardiologists reconstruct the electrical activity of the heart from "boundary" conditions, i.e. skin-detected electrical activity in the form of an ECG, EIT reconstruction methods give a conductivity pattern inside the region that maps into boundary values. When the calculated skin values—calculated from the supposed internal pattern—map into values very similar to the one actually measured in real life, then the supposed pattern is given as the tomographic reconstruction.

Let V be the boundary values, resulting of an unknown mapping U , which is a function of the injected currents I and the conductivity distribution s , then:

$$V = U(s, I)$$

The Jacobian matrix J is somehow a derivative dV/ds which if inverted could help determine the distribution s . But it is not possible because the procedure is an "ill-conditioned problem", i.e. little noise in the measured data lead to unacceptable errors in the reconstructed conductivity. To overcome the ill-conditioning, a method is needed and one is the Tikhonov regularization.

4.6.2 First Part of the Solution: Forward Problem-Solving

To solve the inverse problem, it is necessary to know the forward problem, which is the mapping of the conductivity inside the body to the potentials along the boundary. Since it is a non-linear mapping, we assume there must be a linear equivalent. The determination of the forward operator by mathematical analysis is only possible if the geometry and the conductivity of the EIT problem are simple (e.g. uniform conductivity in a cylinder) (Saulnier 2004). In all other cases, it is necessary to numerically discretise both the region and the conductivity with finite elements. It is also necessary to feed the method with initial experimental data to obtain a linear formula. For the saline-filled tank, a circular geometry is acceptable, while for chest reconstruction it must be replaced by closer anatomical approximations, sometimes adapted to the size and age of the patient.

4.6.3 Second Part of the Solution: Regularization

The inverse problem consists in determining the parameters m corresponding to the measurements d knowing the mapping H . The measurement errors and uncertainties involved are such that in practical terms, it does not hold. This is called an ill-conditioned problem in Hadamard's sense (Borsic et al. 2007) which implies that at least one of the following is true:

1. The solution does not exist.
2. The solution is not unique.
3. The solution is a noncontinuous function of the data, such that small data perturbations cause arbitrarily large errors in the reconstructed parameters.

The Tikhonov method confines the solution to a space of expected solutions: this is done by adding a term introducing information about where the solution might be, starting from an initial estimation. Different modifiers can be used, such as Tikhonov's standard regularization or NOSER's regularization which takes into account an initial conductivity estimate (Santos 2014).

4.7 Comparison of Reconstruction Implementations

To obtain a tomographic reconstruction, we consider three different implementations: the original IMPETOM (Hartman et al. 2002) and GREIT and NOSER regularizations, both obtained using the EIDORS package (Borsic et al. 2007) which is an open-source software suitable for EIT image reconstruction with several algorithms to solve both forward and inverse problems. IMPETOM original reconstruction software uses the Newton-Raphson method with finite elements (Hartman et al. 2002).

4.7.1 *Phantom and Volunteer Experimental Data*

The original data was obtained using IMPETOM circuitry (Gonzalez et al. 2005) and was tested with both the IMPETOM system and EIDORS (EIDORS: Electrical Impedance Tomography and Diffuse Optical Tomography Reconstruction Software (Version 3.5)). This comparison is important for prototype development and deciding the best algorithm to adopt.

For development purposes an original cylindrical tank phantom was build. It consists of a cylindrical tank 21 cm in diameter, filled with saline solution. Inside the tank an empty 8 cm diameter plastic bottle was initially moved along a diameter of the tank and subsequently around its boundary (Ferreira 2002).

A healthy volunteer was harnessed with the 16 electrodes of IMPETOM to image his chest (Gonzalez 2005).

A/D converter of IMPETOM allowed to acquire images at a rate of 15 frames per second. The experiment with the phantom included 300 frames; 400 frames of the volunteer were acquired.

4.7.2 *GREIT Reconstruction Algorithm*

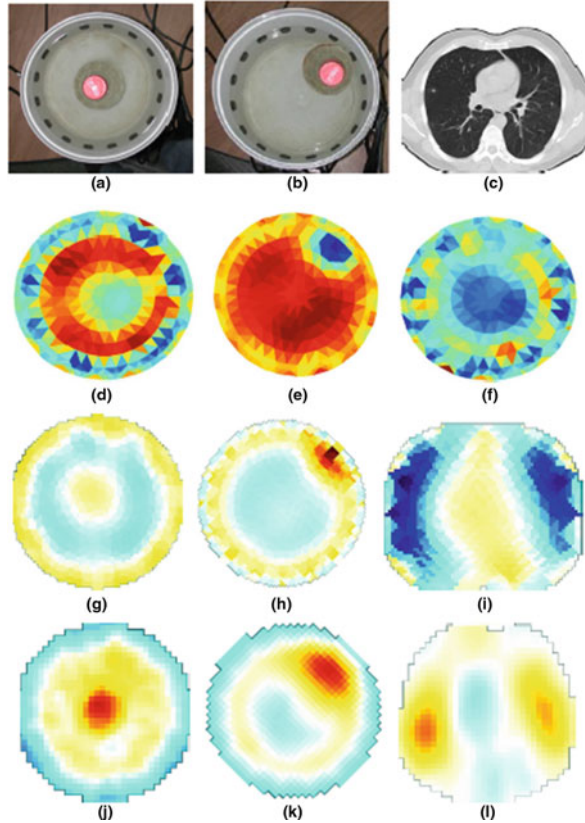
We used the GREIT “Graz consensus linear Reconstruction algorithm for lung EIT” (Adler et al. 2009). The specifications of GREIT are:

1. Single-ring electrode configurations with adjacent current injection and measurement.
2. Linear reconstruction of a 2D conductivity difference image, based on a forward model, which allows real-time processing.
3. Reconstruction into a 32 by 32 pixel array for a single ring of 16, 12 or 8 electrodes.
4. Predefined shapes of (a) neonatal chest, (b) male and female adult chest and (c) cylindrical tank.

GREIT is useful because it includes performance figures of merit for EIT image reconstructions (Adler et al. 2009). Consensus figures of merit, in order of importance, are:

1. Uniform amplitude response.
2. Small and uniform position error.
3. Small ringing artefacts.
4. Uniform resolution.
5. Limited shape deformation.
6. High resolution.

Fig. 4.4 Comparison of reconstruction methods: the first row shows the phantom or patient to be imaged. The lines below show the output of IMPETOM (492 pixels), NOSER (equivalent to 2048 pixels) and GREIT (1024 pixels) algorithms. The first column is an empty plastic bottle in saline. The second column shows the bottle placed near the edge of the tank. The third column is a sample CT scan and tomographic sections of a normal volunteer



4.7.3 Comparison of Reconstructions

Standard IMPETOM parameters were used: 492 elements, 2D circular mesh. Regularization NOSER parameter was set by trial and error to 0.07 for phantom imaging (Fig. 4.4g, h) and to 1.0 for the healthy volunteer (Fig. 4.4i). For the cylindrical phantom, 256 element 2D circular mesh was used. A thorax-shaped mesh was selected for the volunteer. The GREIT algorithm was trained with a uniform distribution of points for the chest and a heavy-centred distribution of points (Hamidi et al. 2010) for the phantom. The initial image for the cylindrical tank is a uniform circle which gives a frame for simulated measurements with the forward solution. The frame difference was then used to feed the inverse problem in order to obtain tomographic sections (Fig. 4.4). The initial frame is the mean of 400 real skin measurements. The difference between the mean frame and the real frame is fed to the inverse problem algorithm producing the tomographic image.

The results of reconstructions are shown in Fig. 4.4. Considering that our goal was to develop a prototype for quantitative air/fluid chest distribution (Santos and Simini 2012) and not an anatomically accurate image, the results are promising.

IMPETOM Fig. 4.4d, e, f were not as good as GREIT Fig. 4.4j, k, l but were better than NOSER Fig. 4.4g, h, except for the lung reconstruction in Fig. 4.4i. With standard desktop computing power, all three methods create images in less than a second. The GREIT algorithm included a 3D mesh to account for current leakages to adjacent planes, which is a factor of quality. There are two details that will enable to obtain better results for chest reconstruction (Fig. 4.4i, l) with respect to the original IMPETOM prototype (Fig. 4.4f): a chest-shaped model and starting with the mean of 400 frames to feed the inverse problem-solver.

4.8 EIT Using a Standard Board

Evaluation module OMAP-L137 from Spectrum Digital can be used as the core part of an EIT system. Its audio codec AIC3106 is used as a signal generator and to perform voltage measurements, with the included DSP C6747 from Texas Instruments for data processing.

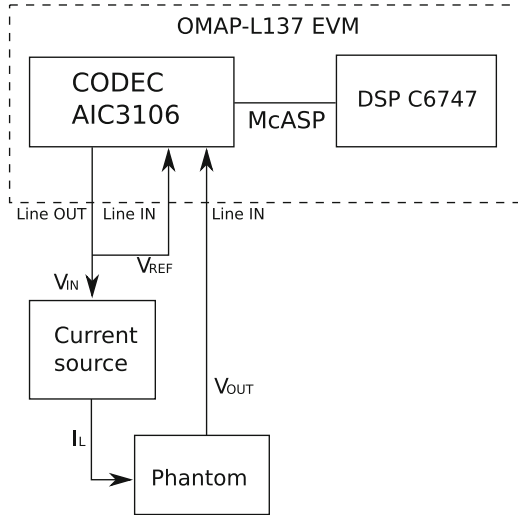
The evaluation module (EVM) is an independent platform that allows developing and studying several applications for the OMAP-L137 integrated circuit. It has incorporated a multicore system on chip (SoC) that permits to work simultaneously the two processors nested within: the floating-point digital signal processor (DSP) C6747 VLIW with 32 bits, running at 300 MHz, and the RISC processor ARM926EJ-S also running at 300 MHz (both from Texas Instruments). Besides, the EVM has a series of microcontrollers, peripherals, inputs and outputs for diverse purposes. The audio codec AIC3106 has two separate input channels with a resolution of 24 bits and 48 kHz sampling rate, a multichannel serial port McASP, stereo inputs and outputs Line IN and Line OUT and 32 megabytes of SDRAM.

The system we implemented has a 16 kHz digital sine wave generated using a table within the DSP, which is sent to the audio codec through the serial channel McASP. The internal digital-to-analog converter (DAC) in the AIC3106 transmits the converted signal through the Line OUT port. The voltage signal V_{in} feeds a Howland current source, whose output impedance depends upon resistor matching and non-linearities.

Input signals to the audio codec VREF and VOUT are amplified by a programmable gain amplifier (PGA). Then signals pass through an antialiasing filter. Resultant signals are converted to digital samples at a sample rate of 48 kHz by means of an ADC. These samples are sent from AIC3106 to DSP C6747 through the McASP channel. A synchronous demodulator is implemented in the DSP to obtain the real part of the voltage VOUT. After digitizing, both input signals are multiplied sample by sample and inverted (since the current source has an inverter configuration). The real part of VOUT is proportional to the DC component of the resulting signal. An infinite impulse response (IIR) filter is used to filter the signal and the result is the DC component.

In order to test the audio codec behaviour as ADC input channel, we used a Tektronix CFG253 signal generator directly connected to one of the Line IN

Fig. 4.5 Block diagram of an EIT system implemented with the evaluation module (EVM) OMAP-L137 and an external current source. Taken with permission from Alfaro et al. (2016)



channels in the EVM. The sinusoidal input signals were simultaneously measured with oscilloscope Tektronix TDS210. The results show a linear response from the codec with differences under 5% for values in the range from 42 mV to 1.5 V (Alfaro et al. 2016).

The system in Fig. 4.5 was then implemented with a Howland current source. A RC parallel circuit worked as our load impedance: a 100 nF capacitor placed in parallel with a variable resistor. An algorithm to obtain the real part of the impedance was implemented in the DSP, given the linearity between V_{ref} and the current generated. By comparing the estimated real part calculated by the DSP with the oscilloscope, it was noticed that the EVM responds correctly to changes in the load impedance and the mean difference between values was 8.5% (every measurement was repeated five times to assess repeatability, giving 0.3% mean deviation).

The EVM (OMAP-L137) module with audio codec AIC3106 has proven to be suitable as an EIT system core. Since measurements are reliable above 42 mV, improving the current source is essential and should be such as to have a 42 mV effect for the smallest bioimpedance to be detected (Fig. 4.6).

4.9 Electrical Phantom to Test EIT Systems

Before using circuits on volunteers, we designed a simple saline-filled tank such as the one in Fig. 4.7, as a test phantom. This allows to perform qualitative tests. But we also need detailed calibration tests. Since most of the information is derived from the real part of the impedance values measured on a patient, but there is also a capacitive component, we decided to simulate a simple measurement by connecting a phantom made of a resistance $R = 350$ to $R = 600$ ohm in parallel with a capacitor of $C = 47$ nF. This circuit is fed by the modified Howland current

Fig. 4.6 Connection diagram of the test bench. The modified Howland current source feeds a phantom (parallel RC: $C = 47$ nF and a variable resistor). The oscilloscope allows to compare the original codec voltage signal to the phantom-shaped voltage. Taken with permission from Arregui et al. (2016)

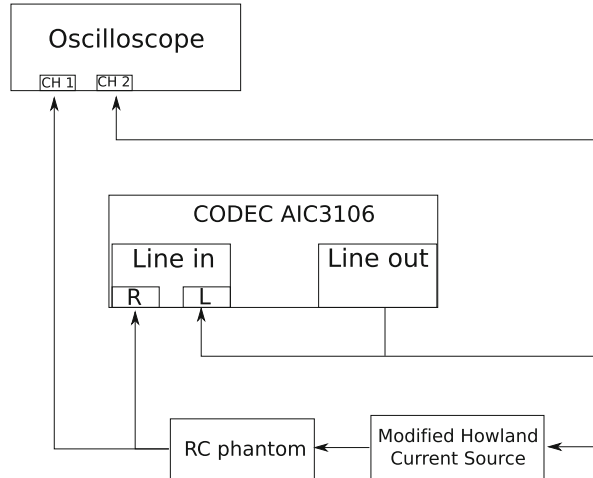


Fig. 4.7 Test tank with three electrode rows for saline solution. After Quinteros and Simini (2007) with permission



source (Saulnier 2004) controlled by one of the codec output signals, proportional to a DSP-originated 16 KHz sinusoidal wave. We suggest to include the test RC “phantom” within the actual EIT instrument, to be available as “self-test” or “self-calibration”.

The codec was configured to work with a 48 kHz sampling frequency in slave mode, and the data transfer protocol was “I2S to DSP” and 16-bit word length. No offset is added to the data. The PGA gain of each channel was set to 0 db. Communication between DSP and codec is through McASP serial port communication settings synchronized with two-slot TDM format.

The current source of 16 KHz (in addition to give rise to currents to be injected) is measured by the oscilloscope, as a phase reference for all current measurements. The same oscilloscope is also connected to the output of the RC phantom and to the input of the current source, where the voltage is in phase with the current injected

Table 4.1 Real part of the RC phantom and relative error

| R Phantom (Ω) | Impedance R//C real part @ 16 KHz (Ω) | Oscil. measurement (Ω) | IMPETOM measurement (Ω) | IMPETOM adjusted R//C (Ω) | Relative error (%) |
|------------------------|--|---------------------------------|----------------------------------|------------------------------------|--------------------|
| 350 | 93.7 | 107.6 | 108.3 | 92.6 | 1.23 |
| 400 | 87.5 | 111.3 | 104.5 | 88.2 | 0.82 |
| 450 | 81.5 | 101.3 | 98.8 | 81.8 | 0.38 |
| 500 | 76.0 | 94.7 | 94.6 | 77.1 | 1.43 |
| 550 | 70.9 | 85.5 | 88.7 | 70.4 | 0.74 |
| 600 | 66.4 | 78.9 | 84.7 | 66.0 | 0.66 |
| Average error | | | | | 0.876 |

into the phantom. This allows to compare measurements made by the EIT system with a reliable instrument such as a laboratory oscilloscope.

The 2016 IMPETOM software uses the phase of the reference voltage signal to compare it to the phase of the resulting phantom voltage. The output voltage signal of the phantom circuit allows to calculate the real part of the phantom impedance. We do not use as a time reference the original DSP generated signal which is fed to the codec to control the current source, because it would introduce a lag from the time the DSP sends the signal to the time the codec effectively outputs the signal at its output channel. To avoid this delay, we use a second codec input channel to measure the signal of its own output port. In this way we reduce the time overhead derived from causes other than the phase change to be measured. Sampled signals and data are then sent from the codec to the DSP. We have tested our circuit with several values of R and a fixed C value, all reported in Table 4.1.

In our previous IMPETOM designs, time control was performed by a single analog signal multiplexed into 16 current sources. But when a decision was made to use digital circuits and audio kits to cut development costs, real part impedance measurement errors became high. Debugging gave as a result an unexpected phase lag between signals. An internal digital signal, given by the manufacturer as a vector in codec memory, was initially used as a reference to measure real-world hardware signal phases, but this also produced uncontrolled errors. A way to overcome this difficulty in future designs is to use the same codec-generated D/A signal as a reference for measurement as well as to create the signal to submit to the “patient simulator” or phantom, with reliable measurement values to be expected. This was actually the case, and thus the inclusion of the “phantom” with variable R and fixed C can be of help during development as well as a “self-test” feature of prototypes and future instruments alike. An error of 1% was measured, which is a reliable enough test bench to let prototypes inherit the precision of laboratory instruments. Without the “RC phantom”, the impedance real part would be estimated with large errors due to lack of common time reference. This special measurement requirement is necessary because modern designs include software signal generation, as opposed

to traditional layouts with a central analog oscillator to command all current sources. Future additional enhancements could be the inclusion of measuring bridges to improve sensitivity and 32-bit digital encoding to reduce quantification errors.

4.10 Current Leakage to Adjacent Chest Sections

EIT consists of current injection along a line on the skin of the patient and voltage measurements taken at the same electrodes. The assumption that all injected current is confined to the section under study, i.e. the section defined by the electrodes, is plausible but should be confirmed.

A first set-up with three rows of electrodes on the sides of a saline-filled tank is shown in Fig. 4.7. Similar to the “one row phantom tank” in all aspects, this phantom allows both to inject current in 16 electrodes and to measure 48 voltages (actually 46, since the two injecting electrodes are not used simultaneously). The distance from the central to the adjacent sections is 5 cm, which can eventually allow to measure voltage induction up to 10 cm away by “stimulating” either the top or bottom row. The EIT images of cylindrical empty bottles obtained were very similar irrespective of the row at which the voltages were measured, using the IMPETOM system (Quinteros and Simini 2007).

Manufacturers of real-time EIT system (Dräger 2011) publish estimated distributions of current away from the injection section which fade away to 10% at 10 cm of the central section.

4.11 Discussion and Conclusion

At a time of growing investment in health and of increasing concern on ionizing radiation, “soft” instrumentation such as EIT has the potential of a great development and adoption in clinical settings. Surprisingly only a small fraction of the effort devoted to classical imaging technology such as MRI, CT and PET is published in bioimpedance under all its forms, spectroscopy, EIT, organ composition analysis or new applications. This chapter contains clear evidence that sound electronics and mathematical methods can be successfully applied to EIT development and testing to match the clinical need of simple reliable fluid occupancy monitoring of intensive care patients. Thirty years have passed since the initial work of the Sheffield group to commercial dissemination in an incipiently meaningful proportion of medical units. All is set for EIT to fully occupy its market share for critically ill patient management in the coming years.

Acknowledgements Interest in electrical bioimpedance and motivation to develop EIT systems was originated by a clinical request by Professor Javier Hurtado and associates Dr. Walter Olivera and Dr. Cristina Santos in 1986, at that time active in the foundation of the Pulmonary

Functional Testing Laboratory of the University Hospital of Uruguay. Pioneering work by Dr. Fernando Nieto—prematurely deceased 2001—with one of the authors gave as a result our first bioimpedance spectroscopic tetra-electrode instrument in 1994 which prompted us to tackle the development of an EIT device with successive prototype versions. Editorial assistance with intensive care insight and counselling by Dr. Bruno Simini of Ospedale di Lucca, Italy, was very much appreciated and is greatly thanked for. The work of the following students since 1994 is acknowledged here: Cecilia Frugoni, Ramiro Escuder, Lauro Artía, Raúl Hartman, Jorge Lobo, Mateo Ruétalo, Adriana Ferreira, Alfredo Rodríguez, Santiago González, Andrés Liguori, Walter Quinteros, Nicolás Alfaro and Fernanda Martinucci. Special thanks are due to Professor Roberto Markarian and to Dr. Pablo Musé for their interest and suggestions during their 2013 graduate course on Real and Functional Analysis. Several colleagues have given substantial help to this work including, but not limited to, Pablo Mazzara, Rafael Canetti, Linder Reyes and Daniel Geido.

References

- Adler, A., et al. (2009). GREIT: A unified approach to 2D linear EIT reconstruction of lung images. *Physiological Measurement*, 30(6), S35–S55.
- Alfaro, N., Arregui, M., Martinucci, F., Santos, E., & Simini, F. (2016). Audio codec and digital signal processor for an electrical impedance tomography system. In *II Lat. Am. Conf. Bioimpedance, CLABIO 2015* (pp. 16–19).
- Arregui, M., Santos, E., & Simini, F. (2016). Test bench to validate audio codec kit as EIT complex voltage measurement circuit. In *VII Latin American Congress on Biomedical Engineering CLAIB 2016, Bucaramanga*.
- Barber, D. C., & Brown, B. H. (1984). Applied potential tomography. *Journal of Physics E: Scientific Instruments*, 17, 723–733.
- Bera, T. K., & Nagaraju, J. (2009). A Simple instrumentation calibration technique for Electrical Impedance Tomography (EIT) using a 16-electrode phantom. In *Automation science and engineering, 2009. CASE 2009. IEEE International Conference on* (pp. 347–352).
- Borsic, A., Graham, B., Adler, A., & Lionheart, W. (2007). *Total variation regularization in electrical impedance tomography* (techreport). Manchester, UK.
- Dräger. (2011). PulmoVista 500 Data Sheet.
- EIDORS: Electrical Impedance Tomography and Diffuse Optical Tomography Reconstruction Software (Version 3.5).
- Ferreira, A., Rodríguez, A., & Simini, F. (2002). *IMPETOM-C Tomógrafo de Impedancia Eléctrica*. Academic thesis, Universidad de la Republica, Montevideo.
- Gaggero, P. O., Adler, A., Brunner, J., & Seitz, P. (2012). Electrical impedance tomography system based on active electrodes. *Physiological Measurement*, 33(5), 831.
- Gonzalez, S., Liguori, A., & Simini, F. (2005). *IMPETOM Academic thesis*.
- Hamidi, S. A., Jafari, R., Nia, A. M., & Soleimani, M. (2010). Design and implementation of a DSP-based digital phase sensitive demodulation for an EIT system. *Journal of Physics Conference Series*, 224(1).
- Hartman, R., Lobo, J., Ruétalo, M., & Simini, F. (2002). *IMPETOM-I Tomógrafo de Impedancia Eléctrica*. Academic thesis, Universidad de la Republica, Montevideo.
- Quinteros, W., & Simini F. (2007) *IMPETOM-48 Tomógrafo de Impedancia Eléctrica con tres hileras de electrodos*. Academic thesis, Universidad de la Republica, Montevideo.
- Santos, E. (2014). *Alternativas de proyecto tendientes a un tomógrafo por impedancia eléctrica para la presentación del estado edemático en tiempo real*. Tesis Maest, Univ. la República, Uruguay, p. 199.
- Santos, E., & Simini, F. (2012). Electrical impedance tomography for pulmonary oedema monitoring: Review and updated design. *Journal of Physics Conference Series*, 407, 12024.

- Santos, E., & Simini, F. (2013). *Comparison of EIT reconstruction techniques applied to IMPETOM*. 13th International Conf. Bioinformatics and Bioengineering, Chania, Greece
- Saulnier, G. (2004). EIT instrumentation. In D. Holder (Ed.), *Electric impedance tomography: Methods, history and applications* (p. 65). London: IOP Publishing.
- Soleimani, M. (2006). Electrical impedance tomography system: An open access circuit design. *Biomedical Engineering Online*, 5(28).
- Swisstom, A. G. Swisstom EIT System.
- Wang, C., Liu, J., & Wang, H. (2005a). Pipeline data acquisition method in the EIT system. In *Instrumentation and measurement technology conference, 2005. IMTC 2005. Proceedings of the IEEE* (Vol. 1, pp. 437–440).
- Wang, M., Ma, Y., Holliday, N., Dai, Y., Williams, R. A., & Lucas, G. (2005b). A high-performance EIT system. *Sensors Journal, IEEE*, 5(2), 289–299.
- Webster, J. (2010). *Medical instrumentation. Application and design*. Hoboken, NJ: Wiley.
- Xu, G., Zhang, S., Wu, H., Yang, S., Geng, D., Yan, W., et al. (2005). The acquisition hardware system with direct digital synthesis and filtered back-projection imaging in electrical impedance tomography. In *Engineering in medicine and biology society, 2005. IEEE-EMBS 2005. 27th Annual International Conference of the* (pp. 7758–7761).